RSC Advances




ROYAL SOCIETY OF CHEMISTRY

www.rsc.org/advances

RSC Advances

ARTICLE

# Synthesis and Photovoltaic Properties of A-D-A Type Non-fullerene Acceptors Containing Isoindigo Terminal Units

Xin Liu, Yuan Xie, Xinyi Cai, Yunchuan Li, Hongbin Wu, Shi-Jian Su* and Yong Cao

Received 00th January 20xx,
Accepted 00th January 20xx

DOI: 10.1039/x0xx00000x

www.rsc.org/

Four solution-processable acceptor-donor-acceptor (A-D-A) structured organic molecules with isoindigo as terminal acceptor units and different aromatic rigid planar cores such as indacenodithiophene (IDT), dithienosilole (DTS), anthracene, and pyrene as donor units, namely P1, P2, P3, and P4, respectively, were designed and synthesized as the acceptor materials in organic solar cells (OSCs). The four compounds possess a broad absorption covering the wavelength range of 400–700 nm and a rather high-lying LUMO energy level, which is beneficial for achieving a high open circuit voltage ($V_{oc}$). P1 and P2 with IDT and DTS central cores demonstrate stronger absorbance than the compounds P3 and P4 with anthracene and pyrene cores. Power conversion efficiency (PCE) of 1.39% was achieved for the OSCs based on P1 as the acceptor material and P3HT as the donor material (1:1, w/w), which is the highest value for the polymer bulk-heterojunction OSCs based on isoindigo small molecules as non-fullerene acceptors. The current results have demonstrated that isoindigo could be a useful building block for the synthesis of promising acceptor materials for OSCs.

## Introduction

Conventional bulk-heterojunction (BHJ) organic solar cells (OSCs) are based on polymer or small molecule materials as electron donor and fullerene derivatives as electron acceptor [1-5]. Compared with inorganic solar cells, OSCs are made with non-toxic and cheap materials and are manufactured by low cost technologies such as solution process or roll-to-roll process on large areas of light-weight flexible substrates [6-7]. The performance of the fullerene based OSCs has also been improving steadily with power conversion efficiencies (PCEs) surpassing 10% for single junction OSCs [8-10]. Despite the essential role of fullerene derivatives in achieving best performance OSCs, fullerene acceptors have several drawbacks including poor light absorption, high-cost production and purification [11-12]. For this reason, OSCs based on small molecular non-fullerene acceptors have attracted much attention due to the easy adjustment of electronic and optical properties of non-fullerene acceptor materials and have been improving progressively during the past few years. There have been many reports of non-fullerene-based OSCs [13-14] achieving PCEs ranging from 3-5% until a recent report of PCE passing 6% [15-27].

Donor-acceptor (D-A) framework molecules are widely used in small molecular donor materials for BHJ OSCs and obtained excellent PCEs. Donor-acceptor chromophores involving electron-donating and electron-accepting moieties have been extensively investigated for small molecular donor materials for BHJ OSCs [28]. Well-chosen donor and acceptor groups are particularly desirable for low band-gap materials due to a significant enhancement of the intramolecular charge transfer (ICT) intensity and conjugation length, which lead to a better extended absorption and higher absorption coefficient [29]. Furthermore, the HOMO and LUMO energy levels can be tuned through designing different central donor moiety and two conjugated electron-accepting moiety on both sides. It is thus expected that great improvement could be made to the photovoltaic performance for small molecular non-fullerene acceptors with A-D-A structure through delicate chemical structure design and modification. With the performance of OSC devices entering the realm of potential commercial application, the design of organic electronics is becoming increasingly focused on materials that can be synthesized from sustainable and readily available building blocks.

Isoindigo (II) is a naturally occurring isomer of the largest textile dye in the world, and that is found in the leaves of Isatis tinctoria [30-32], which can be effectively synthesized in bulk quantities, allowing the preparation of numerous II-based donor materials with promising performance in organic electronics [31, 33-38]. It has the inherent characteristics of the strong electron-withdrawing, relatively narrow band gaps and planar structures [39-44]. II is composed of two symmetrical oxindole rings that are connected with each other through 3-carbon unsaturated double bond, which effectively

*State Key Laboratory of Luminescent Materials and Devices and Institute of Polymer Optoelectronic Materials and Devices, South China University of Technology, Guangzhou 510640, P. R. China E-mail: mssjsu@scut.edu.cn; Fax: +86 2087110606; Tel: +86 20 22237098.*
† DOI: 10.1039/x0xx00000x

binds two electron-withdrawing carbonyls and two electron-rich phenyl rings in a trans-conformation. This formation has a donor–acceptor–donor type system with fully delocalized highest occupied molecular orbital (HOMO) and localized lowest unoccupied molecular orbital (LUMO) at the electron-withdrawing lactam rings [36]. Regarding electronic and structural properties, II offers an extended absorption towards the near-IR with LUMO energy level of -3.9 eV and high optical stability [44].

In this article, four small molecules (**Scheme 1**) with A-D-A framework comprised of aromatic rigid fused rings including indacenodithiophene (IDT), dithienosilole (DTS), anthracene, and pyrene cores as the donors, which have been widely applied in the construction of high-mobility organic semiconductors because the extended conjugation in fused ring is beneficial to forming effective intermolecular π-π overlaps and thus enhanced carrier transport, two II units as the acceptor were designed and synthesized as the platform for investigating the effect of the different cores. Two II electron-withdrawing acceptor units which can lower the LUMO energy levels since the π* energy of the electron-withdrawing unit can be efficiently mixed, leading to stabilization of the LUMO, are linked with the different electron donor core, leading to intramolecular charge transfer and thus broad optical absorption. While, to the best of our knowledge, there are a few publications that report on isoindigo-based small molecular non-fullerene acceptors in bulk heterojunction solar cells [45-47]. The developed materials show good solubility in common organic solvents, such as chloroform (CF), dichloromethane (DCM), tetrahydrofuran (THF), chlorobenzene (CB), 1,2-dichlorobenzene (DCB), and toluene, and can be readily solution-processed to form smooth and pinhole-free films upon spin-coating. Small molecular BHJ OSCs were fabricated using these materials as the acceptor and P3HT as the donor. The device based on P3HT and P1 displays a relatively high PCE of 1.39% with an open circuit voltage ($V_{oc}$) of 1.05 V, a short circuit current density ($J_{sc}$) of 2.36 mA $cm^{-2}$, and a fill factor (FF) of 0.56. The PCE of 1.39% is the highest value for the polymer BHJ OSCs based on isoindigo small molecules as non-fullerene acceptors.

## Experimental

**General.** $^{1}H$ and $^{13}C$ NMR spectra were recorded on a Bruker AV-500 spectrometer operating at 500 and 125 MHz, respectively, in deuterated chloroform solution at room temperature. MALDI-TOF (matrix-assisted laser-desorption/ionization time-of-flight) spectra were recorded on a Bruker BIFLEX III instrument. Differential scanning calorimetry (DSC) measurements were performed on a Netzsch DSC 209 under a $N_2$ flow at a heating and cooling rate of 10 °C $min^{-1}$. Thermogravimetric analyses (TGA) were performed on a Netzsch TG 209 under a $N_2$ flow at a heating rate of 10 °C $min^{-1}$. UV-Vis absorption spectra were recorded on a HP 8453 spectrophotometer. Photoluminescence (PL) spectra were measured using a Jobin-Yvon spectrofluorometer. Cyclic voltammetry (CV) was performed on a CHI600D electrochemical workstation with a platinum working electrode and a Pt wire counter electrode at a scanning rate of 100 mV $s^{-1}$ against a $Ag/Ag^{+}$ (0.1 M of $AgNO_3$ in acetonitrile) reference electrode with an argon-saturated anhydrous acetonitrile solution of 0.1 M tetrabutylammonium hexafluorophosphate. Thin solid films used for UV-vis absorption and PL spectral measurements were prepared by spin-coating their *o*-dichlorobenzene solutions on quartz substrates. Atom force microscopy (AFM) measurements were carried out by using a Digital Instrumental DI Multimode Nanoscope IIIa in tapping mode. The processing conditions to make the blend films for morphology study are the same as those for the fabrication of the solar cell devices.

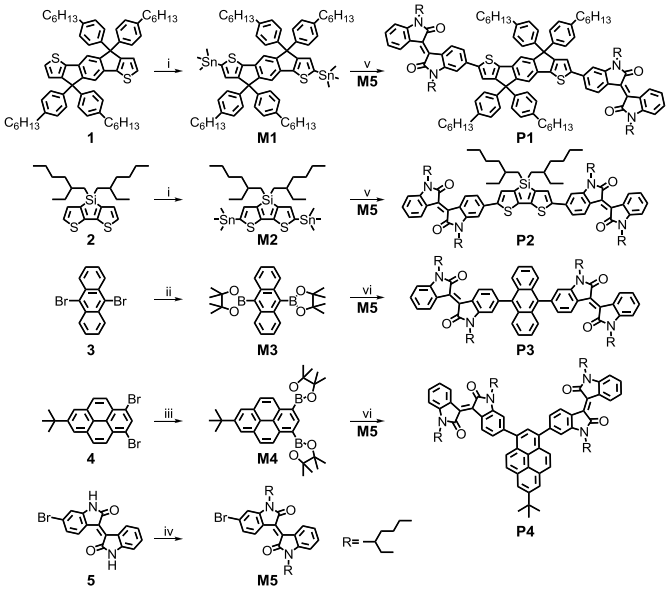


**Scheme 1** Molecular structures and synthetic routes of P1, P2, P3, and P4. *Reagents and conditions*: (i) n-BuLi, THF, 1h, -78℃; $(CH_3)_3SnCl$, -78℃; rt; (ii) $Pd(dppf)Cl_2$, $CH_3COOK$, bis(pinacolato)diboron, 1,4-dioxane, 90℃; (iii) n-BuLi, THF, -78℃, 1h, 2-isopropoxy-4,4,5,5-tetramethyl-1,3,2-dioxaborolane, rt; (iv) 2-ethyl-bromohexane, $K_2CO_3$, DMF, 100℃, 15h; (v) $Pd(PPh_3)_4$, toluene, reflux at 110 ℃, two days; (vi) $Pd(PPh_3)_4$, toluene, $K_2CO_3$, 90℃, two days.

**Materials.** All reactions and manipulations were carried out under inert atmosphere with the use of standard Schlenk techniques. THF was distilled from sodium before use. The other reagents and solvents, unless otherwise specified, were purchased from commercial suppliers and used without further purification. As outlined in **Scheme 1**, the II-based small molecules, P1 and P2, were synthesized by Stille cross-coupling reaction, molecules P3 and P4 were synthesized through Suzuki coupling reaction.

Compound **M1**. n-BuLi (1.1 mL, 2.5 M in hexane) was added dropwise to a solution of compound **1** [48] (1.0 g, 1.1 mmol) in THF (20 mL) at -78℃. The mixture was kept at -78℃ for 30 min and then warmed to room temperature for another 30 min. After cooling to -78℃ again, trimethyltin chloride (2.5 mL, 1 M in hexane) was added. The reaction was stirred overnight at room temperature and then quenched with water, extracted with hexane, and dried over $Na_2SO_4$. After removal of the solvent, ethanol was added to the mixture and the

precipitate was collected as a white solid (**M1**, 1.1 g, 82%). $^1$H NMR ($CDCl_3$, 500 MHz): d (ppm) 7.40 (s, 2H), 7.15 (d, 8H), 7.07 (d, 8H), 7.03 (s, 2H), 2.56 (t, 8H), 1.58 (m, 4H), 1.31 (m, 28H), 0.89 (t, 12H), 0.35 (s, 18H).

Compound **M2**. Compound **2** [49] (1.26 g, 3.00 mmol) was added into a 50 mL flask and purged with Ar under vacuum. 20 ml of dry THF was added into a flask. The solution was cooled down to -78 °C. Then n-BuLi/hexane solution (3.84 mL, 6.14 mmol) was added dropwise. The temperature was then raised to about room temperature, and the solution was stirred for 60 min. The solution was cooled to -78 °C again and 1M trimethyltin chloride/THF (6.98 mL, 6.98 mmol) was added. Then the cooling bath was removed. After being stirred at ambient temperature overnight, 20 mL hexane and 20 mL of $H_2O$ was added with stirring, the water layer was separated, the organic layer was washed with 15 mL of $H_2O$ again and the combined water layers were extracted with 20 mL of hexane. The combined organic layers were washed with water again and then dried with $MgSO_4$. After removal of volatiles, **M2** was obtained and used without any further purification as a sticky pale green oil. $^1$H NMR ($CDCl_3$, 500 MHz): d (ppm) 7.24 (s, 2H), 1.41 (m, 2H), 1.21-1.32 (m, 4H), 1.08-1.21 (m, 12H), 0.92-1.08 (m, 4H), 0.81 (t, 6H), 0.77 (t, 6H), 0.38 (s, 18H).

Compound **M3** [50]. To a 100 mL Schlenk flask were added 9,10-dibromoanthracene (**3**, 4.20 g, 12.5 mmol), bis(pinacolato)diboron (7.75 g, 30.5 mmol), palladium acetate (0.166 g, 0.740 mmol), potassium acetate (7.34 g, 75.0 mmol) and 35 mL of anhydrous N,N-dimethylformamide. The mixture was degassed by gently bubbling argon for 30 min at room temperature. This was then heated at 90°C under argon overnight. The cooled mixture was extracted with dichloromethane, washed with brine, and dried over $MgSO_4$. The crude product was chromatographed on silica using 0-10% ethyl acetate in hexane as eluent to give **M3** as a yellow solid (2.7 g, 50%). $^1$H NMR ($CDCl_3$, 500 MHz): d (ppm) 8.35 (dd, 4H), 7.46 (dd, 4H), 1.58 (m, 24H).

Compound **M4**. 1,3-Bibromo-7-*tert*-butylpyrene [51] (**4**, 4.28 g, 10.3 mmol) was dissolved in THF (100 mL) and n-BuLi (20 mL, 1.6M, 32 mmol) was slowly added at –78°C. After addition, the reaction was stirred for 2 h, then 2-isopropoxy-4,4,5,5-tetramethyl-1,3,2-dioxaborolane (7.0 mL, 34.3 mmol) was slowly added at –78 °C. The mixture was stirred overnight and allowed to room temperature. The reaction was quenched with $H_2O$ (30 mL) and diluted with $CH_2Cl_2$, washed with 20% HCl solution, brine, water, respectively, and dried over $MgSO_4$. The organic layer was filtered and evaporated to dryness, followed by column chromatography on silica gel with dichloromethane/petroleum ether (1:4), followed by recrystallization in hexane to give **M4** as a pale yellow powder (2.9 g) in 55 % yield. $^1$H NMR ($CDCl_3$, 500 MHz): d (ppm) 9.02 (d, 2H), 8.95 (s, 1H), 8.23(s, 2H), 8.13 (d, 2H), 1.59 (s, 9H), 1.50 (s, 24H).

Compound **M5** [52]. To a suspension of 6-bromoisoindigo (**5**, 4.20 g, 10.0 mmol) and potassium carbonate (8.29 g, 60.0 mmol) in DMF (45 mL), 2-ethyl-bromohexane (5.79 g, 30.0 mmol) was injected through a septum under nitrogen. The mixture was stirred for 15 h at 100℃ and then poured into water (200 mL). The organic phase was extracted by $CH_2Cl_2$, washed with brine and dried over $MgSO_4$. After removal of the solvent under reduced pressure, the dark red liquids were purified by silica chromatography, eluting with ($CH_2Cl_2$:hexane = 1:6) to give **M5** (3.95 g, 70 %) as a dark red solid. $^1$H NMR ($CDCl_3$, 500 MHz): d (ppm) 9.04 (d, 2H), 7.14 (dd, 2H), 6.83 (d, 3H), 3.56 (d, 4H), 1.83 (bs, 2H), 1.40-1.24 (m, 16H), 0.88-0.84 (m, 12H).

Compound **P1**. Compounds **M1** (494 mg, 0.4 mmol), **M5** (566 mg, 1.0 mmol), $Pd(PPh_3)_4$ (50 mg, 0.043 mmol), and toluene (20 mL) were added to a three-necked round bottom flask. The mixture was deoxygenated with argon for 30 min. The mixture was refluxed for two days and then cooled down to room temperature. A saturated KF aqueous solution (5 mL) was added and stirred overnight. Water (25 mL) was added and the mixture was extracted with dichloromethane (2 × 50 mL). The organic phase was dried over anhydrous $MgSO_4$ and filtered. After removing the solvent from filtrate, the residue was purified by column chromatography on silica gel using petroleum ether/dichloromethane (1:4) as eluent yielding **P1** as a black solid (586 mg, 78%). $^1$H NMR ($CDCl_3$, 500 MHz): d (ppm) 9.04 (d, 4H), 7.40 (s, 2H), 7.12-7.15 (m, 12H), 7.07 (d, 8H), 7.03 (s, 2H), 6.83 (d, 6H), 3.56 (d, 8H), 2.56 (t, 8H), 1.83 (bs, 4H), 1.58 (m, 4H), 1.40-1.24 (m, 60H), 0.84-0.89 (m, 36H). $^{13}$C NMR (125 MHz, $CDCl_3$): d(ppm) 168.3, 157.74, 153.77, 147.55, 146.3, 142.66, 141.35, 141.15, 134.93, 132.6, 131.3, 130.81, 128.39, 128.10, 126.9, 125.2, 120.6, 117.96, 112.7, 62.33, 44.9, 36.3, 35.79, 32.1, 32.0, 31.8, 31.7, 31.55, 30.2, 29.87, 29.77, 29.5, 29.3, 26.6, 22.89, 22.87, 22.62, 14.32. MS (MALDI-TOF) m/z: calculated for $C_{128}H_{156}N_4O_4S_2$, 1878.76; found, 1878.20.

Compound **P2**. **P2** was synthesized and purified in a similar manner to that of **P1** and was obtained as a dark solid (440 mg, 80%). $^1$H NMR ($CDCl_3$, 500 MHz): d (ppm) 9.04 (d, 4H), 7.24 (s, 2H), 7.14 (dd, 4H), 6.83 (d, 6H), 3.56 (d, 8H), 1.83 (bs, 4H), 1.24-1.41 (m, 38H), 0.92-1.21 (m, 16H), 0.77-0.88 (t, 36H). $^{13}$C NMR (125 MHz, $CDCl_3$): d(ppm) 168.2, 155.2, 153.2, 146.3, 141.8, 135.7, 132.6, 131.3, 126.9, 126.2, 125.2, 121.7, 120.6, 113.2, 112.7, 53.8, 44.9, 39.1, 36.3, 32.1, 32.0, 31.7, 30.2, 29.87, 29.77, 29.5, 26.6, 24.3, 22.89, 22.87, 14.34, 14.31. MS (MALDI-TOF) m/z: calculated for $C_{88}H_{118}N_4O_4S_2Si$, 1388.12; found, 1387.79.

Compound **P3**. Compounds **M3** (172 mg, 0.40 mmol) and **M5** (566 mg, 1.0 mmol) were placed in a dried round bottom flask under protective gas. 10 ml of toluene and aqueous potassium carbonate solution (2 M, 5 ml) were added to the flask which then was sealed and degassed with argon for 15 min. Then $Pd(PPh_3)_4$ (10 mg) was added and the solution was heated to 90℃. The reaction mixture was stirred for two days at 90℃. The crude product was obtained by extraction with $CH_2Cl_2$, and the organic phase was subsequently washed with a diluted hydrochloric acid, water and sodium carbonate solution. The organic phase was dried over magnesium sulfate and filtered. The filtrate was concentrated on a rotary evaporator. After the removal of solvent, the crude product was purified by silica gel using a mixture solvent of hexane-dichloromethane as an eluent and afford **P3** as a black solid (390 mg, 85%). $^1$H NMR ($CDCl_3$, 500 MHz): d(ppm) 9.04 (d, 4H), 8.35 (dd, 4H), 7.46 (dd,

4H), 7.14 (dd, 4H), 6.83 (d, 6H), 3.56 (d, 8H), 1.83 (bs, 4H), 1.40-1.24 (m, 32H), 0.88-0.84 (m, 24H). $^{13}$C NMR (125 MHz, $CDCl_3$): d(ppm) 168.2, 146.3, 134.91, 132.6, 131.3, 128.78, 126.9, 125.2, 125.13, 120.6, 112.7, 84.44, 44.9, 36.3, 32.1, 32.0, 31.7, 30.2, 29.87, 29.77, 29.5, 26.6, 25.18, 22.89, 22.87, 14.34, 14.31. MS (MALDI-TOF) m/z: calculated for $C_{78}H_{90}N_4O_4$, 1147.57; found, 1147.10.

Compound **P4**. **P4** was synthesized and purified in a similar manner to that of **P3** and was obtained as a dark solid (392 mg, 80%). $^1$H NMR ($CDCl_3$, 500 MHz): d(ppm) 9.04 (d, 4H), 9.02 (d, 2H), 8.95 (s, 1H), 8.23( s, 2H), 8.13 (d, 2H), 7.14 (dd, 4H), 6.83 (d, 6H), 3.56 (d, 8H), 1.83 (bs, 4H), 1.59 (s, 9H), 1.40-1.24 (m, 32H), 0.88-0.84 (m, 24H). $^{13}$C NMR (125 MHz, $CDCl_3$): d (ppm) 168.2, 148.96, 146.3, 141.75, 138.79, 132.6, 131.3, 131.01, 129.44, 128.34, 126.9, 125.2, 124.32, 123.21, 120.6, 112.7, 84.21, 44.9, 36.3, 35.56, 32.35, 32.1, 32.0, 31.7, 30.2, 29.87, 29.77, 29.5, 26.6, 25.51, 22.89, 22.87, 14.24. MS (MALDI-TOF) m/z: calculated for $C_{78}H_{90}N_4O_4$, 1227.70; found, 1227.77.

**Device fabrication and characterization.** Photovoltaic devices were fabricated with a structure of ITO/ PEDOT:PSS (40 nm)/ active layer (90-100 nm, 1:1, w/w)/ Ca (20 nm)/ Al (80 nm). Indium tin oxide (ITO)-coated glass substrates were cleaned by sonication in detergent, deionized water, acetone, and isopropyl alcohol, and dried in a nitrogen stream, followed by an oxygen plasma treatment. A 40-nm-thin layer of PEDOT:PSS (Baytron P VP AI 4083, filtered at 0.45 μm) was spin-coated (30 s, 3000 rpm) onto the ITO surface. After being baked at 150℃ for 20 min, the substrates were transferred into a nitrogen-filled glove box. Subsequently, a 90-100 nm-thin active layer was spin-casted from the mixture of donor (P3HT) and different acceptor (P1, P2, P3, and P4) in *o*-dichlorobenzene solution (20 mg ml$^{-1}$) at 1500 rpm for 20 s on the ITO/PEDOT:PSS substrate. The active layer thickness was measured using a Dektak 150 profilometer. A 20-nm-thin Ca layer was deposited on top of the active layer. Finally, an 80-nm-thin Al layer was deposited on top of the Ca layer under a high vacuum ($3\times10^{-6}$ torr). The effective device area was patterned to be 0.16 cm$^2$ by using a shadow mask. The PCEs were measured with an AM 1.5G solar simulator (Oriel model 91192) under ambient conditions. The power of the sun simulator was calibrated before the testing using a standard silicon solar cell, giving a value of 100 mW cm$^{-1}$ in the test. The current density–voltage (*J*–*V*) characteristics were recorded with a Keithley 2400 source meter. EQE measurements were conducted using an EQE system (Model QE-R3011, Enlitech Co. Ltd, Kaohsiung, Taiwan). The light source (monochromator, 150W Xe lamp) of EQE system was calibrated by a silicon detector before EQE measurement.

## Results and discussion

**Thermal stability and optical absorption.** The thermal property of the developed materials was investigated by TGA and DSC. The TGA traces reported in **Figure 1** show that P1, P2, P3, and P4 show good thermal stability with decomposition temperatures ($T_d$) of 350, 340, 344, and 370 °C, respectively, as indicated by the temperature corresponding to initial 5% of weight loss in an $N_2$ atmosphere, indicating that they can effectively resist thermal degradation at the operating temperatures in the resultant solar cells. In addition, P4 with pyrene core shows even better thermal stability than the other molecules. The DSC traces for P3 and P4 do not show any peaks from room temperature to 250 °C, indicating that no phase transition was found in this temperature range. However, compound P1 was found to exhibit a melting temperature of approximately 138 °C and a crystallization temperature of approximately 220 °C, respectively, in an $N_2$ atmosphere. Compound P2 exhibits a glass transition temperature of approximately 140 °C (**Figure 2**).

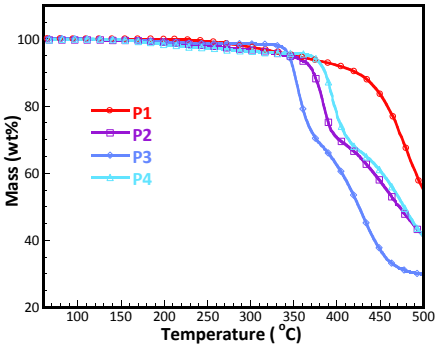


**Figure 1** TGA characterizations of P1, P2, P3, and P4.

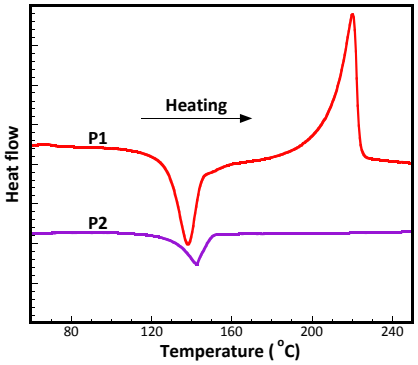


**Figure 2** DSC characterizations of P1 and P2.

To study the relationships between the chemical structure and the photophysical property, UV-vis absorption spectra of P1, P2, P3, and P4 in diluted chloroform solutions ($10^{-5}$ M) and in thin solid films (100 nm) prepared by spin-coating, along with the molar extinction, were recorded as shown in **Figure 3**. Benefited from their A-D molecular structures, the absorption spectra of the compounds in chloroform solutions and thin solid films exhibit a strong and broad absorption band in the wavelength range from 450 to 750 nm. The absorption band at the longer wavelength region could be attributed to the ICT interaction between their donor moieties and acceptor groups [53]. For the four compounds, there is only a small shift in absorption bands, indicating very weak intermolecular interaction in the film state. Compared with the absorption peaks of 506 nm for P3 solution and 503 nm for P4 solution, P1 (587 nm) with IDT core and P2 (613 nm) with DTS core show a large red-shift of about 80-100 nm. The absorption edges of P1, P2, P3, and P4 films are at ca. 780, 782, 650, and 650 nm, respectively, corresponding to optical energy band gaps ($E_g^{opt}$) of 1.59, 1.58, 1.91, and 1.91 eV, respectively, as listed in **Table**

**1**. And compared with compounds P3 and P4, the compounds P1 and P2 show a lower band gap, which can be attributed to stronger electron-donating ability cores and coplanarity between II and its adjacent unit. In addition, P1 and P2 exhibit high absorption coefficients of $4.1\times10^4$ $cm^{-1}$ (619 nm) and $4.6\times10^4$ $cm^{-1}$ (601 nm) in thin solid films, respectively, indicating a very strong solar light absorption ability which is preferable to light-harvesting.

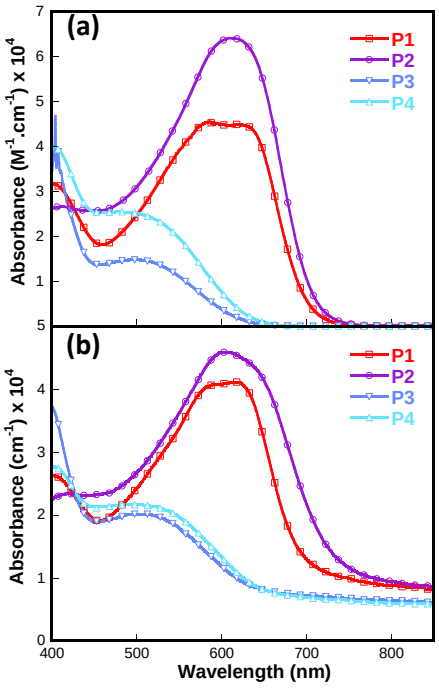


**Figure 3** UV-vis absorption spectra of P1, P2, P3, and P4 in chloroform solutions (a) and thin solid films (b).

**Electrochemical properties and energy levels.** In order to insightfully understand the relationships between the chemical structure and the electronic structure of the resulting materials and consequently provide key parameters for the design of polymer BHJ OSCs, CV experiments were conducted to measure ionization potential (IP) and electron affinity ($E_a$) of P1, P2, P3, and P4. The potentials were calibrated with the redox couple of ferrocene/ferrocenium ($Fc/Fc^+$) under the same experimental conditions. In the oxidation curves shown in **Figure 4**, the CV curves of P1, P2, P3, and P4 in acetonitrile solution show one irreversible p-doping process. The onset oxidation potentials ($E_{ox}$) versus $Ag/AgNO_3$ are 1.25, 1.39, 1.20, and 1.42 V for P1, P2, P3, and P4, respectively. As summarized in **Table 1**, IPs of P1, P2, P3, and P4 are estimated to be 5.66, 5.79, 5.60, and 5.82 eV, respectively, according to an equation of $IP=e(E_{ox}+4.40)$ (eV). Because the reliable onset reduction potentials of these materials are hardly gained, their $E_a$ values are thus estimated from IP and $E_g^{opt}$ to be 4.07, 4.21, 3.69, and 3.91 eV, respectively, based on the relation of $E_a = IP - E_g^{opt}$. The LUMO energy levels of these compounds are close to those of fullerenes, and can match most typical donor materials for OSCs. Because the $V_{oc}$ is proportional to the energy difference between the HOMO energy level of the electron donor and the LUMO energy level of the electron acceptor in the active layer of the BHJ solar cells, such high-lying LUMO energy levels are expected to increase the open circuit voltage in the solar cell devices for P1, P3, and P4.

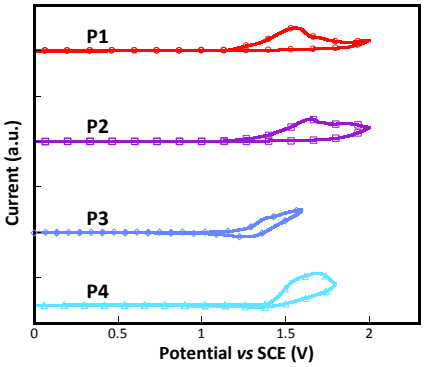


**Figure 4** CV curves of the P1, P2, P3, and P4 films measured in an anhydrous acetonitrile solution of 0.1 M $Bu_4NPF_6$ with a scan rate of 100 mV $s^{-1}$.

**Table 1** Photophysical and electrochemical properties of P1, P2, P3, and P4.

| compound | $\lambda_{max}$ (nm) | | $E_g^{opt\,a}$ | IP[b] | $E_a$[b] | HOMO[c] | LUMO[c] | $E_g$[c] |
|---|---|---|---|---|---|---|---|---|
| | solution | film | (eV) | (eV) | (eV) | (eV) | (eV) | (eV) |
| P1 | 625 | 620 | 1.59 | 5.66 | 4.07 | -4.88 | -2.75 | 2.13 |
| P2 | 614 | 601 | 1.58 | 5.79 | 4.21 | -4.98 | -2.82 | 2.16 |
| P3 | 512 | 510 | 1.91 | 5.60 | 3.69 | -5.18 | -2.72 | 2.46 |
| P4 | 518 | 520 | 1.91 | 5.82 | 3.91 | -5.17 | -2.72 | 2.45 |

[a] Optical energy band gap ($E_g^{opt}$) estimated from the absorption edge of the films ($E_g^{opt}=1240/\lambda_{onset}$).
[b] Electron affinity ($E_a$) calculated from IP and $E_g^{opt}$.
[c] Calculated results of the ground state.

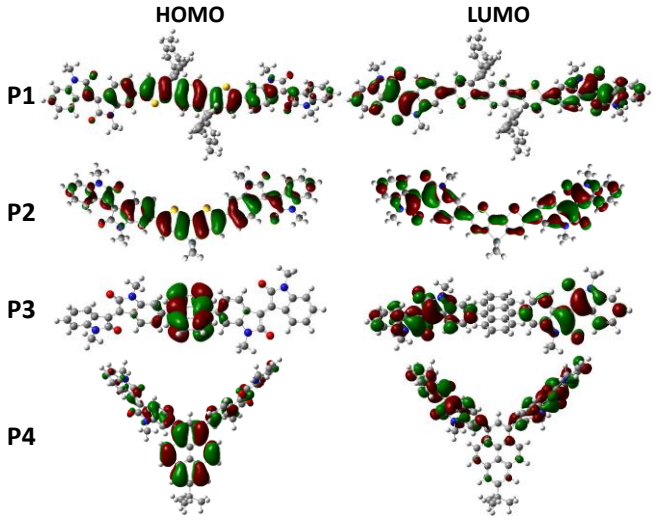


**Figure 5** Frontier molecular orbitals of P1, P2, P3, and P4 based on the optimized geometries (calculated with DFT at the B3LYP/6-31G(d,p) level, Gaussian 03W).

**Theoretical calculations.** To gain further insight into the structure-property relationships of the developed materials at the molecular level, quantum chemical calculations were also performed by using Gaussian 03W program based on B3LYP/6-31G(d,p) basis set to investigate their ground states. To expedite the calculation, the alkyl chains were exchanged with methyl groups to give model compounds. **Figure 5** shows the electron distributions of the HOMOs and LUMOs of the ground-state optimized structures for the compounds. For compounds P1 and P2, the HOMO wave functions are well delocalized along the donor and acceptor units while their LUMO wave functions are more localized at the acceptor parts. In contrast to P1 and P2, the HOMOs of P3 and P4 mainly

locate on the anthracene and pyrene cores, while the LUMOs mostly locate on the II moieties due to its electron-withdrawing ability. It is observed that the electron density of P3 and P4 provides more evident spatial separation of HOMOs and LUMOs than P1 and P2 due to the stronger electron-rich property and better coplanarity of the IDT and DTS cores. Those increased orbital overlap between HOMOs and LUMOs of P1 and P2 contribute to the enhanced absorption coefficient. The calculated HOMO and LUMO energy levels of the ground-state optimized geometries of the compounds are summarized in **Table 1**. LUMO energy levels of these molecules change slightly which is predominantly determined by the acceptor moiety II. However, HOMO energy levels of these molecules change distinctly due to different electron-donating ability of the core and twisted angles of the molecular conformation. The trend of the calculated energy bandgap is consistent with the optical energy bandgaps. The theoretically estimated values refer to the gas phase with isolated molecules, whereas the experimental values are for the condensed phase, and so the values are somewhat different. As shown in **Figure 6**, the twisted angles between the donor and acceptor units are 21°, 20°, 79°, and 51° for P1, P2, P3, and P4, respectively, indicating that the dihedral angles of P3 and P4 increased compared with P1 and P2. The smaller twisted angles of P1 and P2 ensure closely molecular packing, effective intermolecular π-π overlaps, lower band gaps, and thus enhanced charge transport.

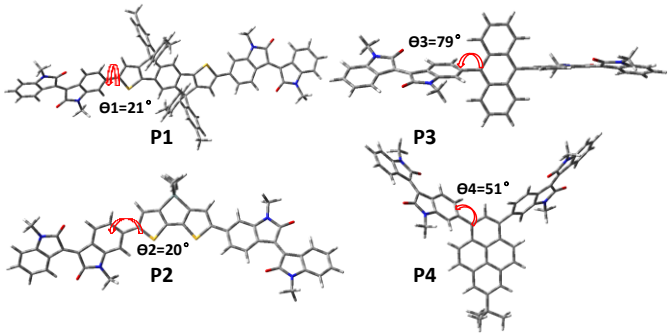


**Figure 6** Twisted angles between the donor and acceptor units of P1, P2, P3, and P4 based on their optimized ground states.

**Photovoltaic properties.** To demonstrate the potential of these small molecules as an electron acceptor material in organic solar cells, photovoltaic devices with a structure of ITO/ PEDOT:PSS (40 nm)/ active layer (90-100 nm, 1:1, w/w)/ Ca (20 nm)/ Al (80 nm) were fabricated by spin-coating from the blend of donor (P3HT) and acceptor (P1, P2, P3, or P4) in an *o*-dichlorobenzene solutions at a concentration of 20 mg $mL^{-1}$. *o*-Dichlorobenzene was used as the processing solvent because it is a good solvent for the developed materials and P3HT. Typical current density-voltage (*J-V*) characteristics of the devices under 1 sun illumination (AM 1.5G, 100 mW $cm^{-2}$) are displayed in **Figure 7**, and the device performances are summarized in **Table 2**. As illustrated in **Figure 7**, both the HOMO offset and LUMO offset between the donor and the acceptors are sufficiently large for photoinduced hole and electron transfer, indicating that the donor-acceptor combination for solar cells is energetically suitable for efficient charge separation. From **Figure 7** and **Table 2**, one can see the characteristically high $V_{oc}$ of the devices based on P1, P3, and P4 (>0.9 V) because of their relatively higher-lying LUMO energy levels. For the conventional devices with P3HT as the donor material without additive and post-deposition annealing of the active layers, the device based on P3HT:P1 with a weight ratio of 1:1 exhibited a very high $V_{oc}$ of 1.05 V, a relatively high $J_{sc}$ of 2.36 mA $cm^{-2}$, an extremely high FF of 0.56, and an outstanding PCE of 1.39%. However, the PCE values of the devices based on P2, P3, and P4 are very low due to very low $J_{sc}$. Compared to the cells based on P3HT:P2, P3HT:P3, and P3HT:P4, the higher PCE of the cells based on P3HT:P1 can be primarily explained by its higher $J_{sc}$ and FF, which possibly results from the broad and strong absorption, excellent planarity and rigid IDT core. In addition, the higher FF (0.56) indicates that P1 has a good miscibility with P3HT to give a favourable donor-acceptor interpenetrating network (IPN). The lower $J_{sc}$ and FF for the devices based on P2, P3, and P4 may be due to an undesirable morphology. It is necessary to note that no additive or thermal annealing was utilized for the current device fabrication, and this is an advantage for simplifying the device fabrication process and improving the repeatability of the device performance.

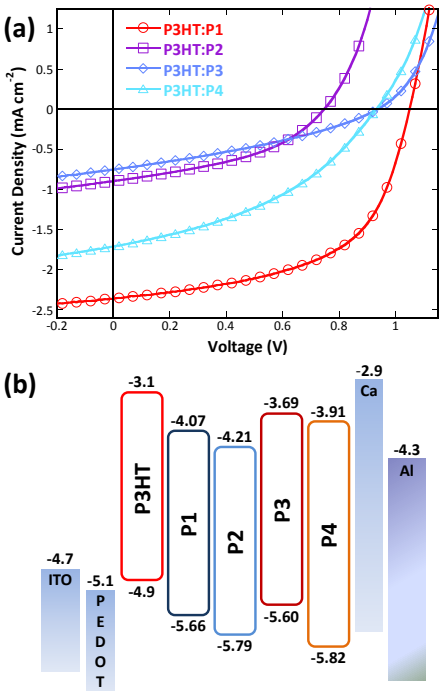


**Figure 7** (a) Current density–voltage characteristics of the OSC devices in a structure of ITO/ PEDOT:PSS (40 nm)/ active layer (90-100 nm, 1:1, w/w)/ Ca (20 nm)/ Al (80 nm) based on an active layer of P3HT:P1, P3HT:P2, P3HT:P3, and P3HT:P4 under the illumination of AM 1.5G, 100 mW $cm^{-2}$; (b) Schematic energy levels of the devices.

**Table 2** Summary of the device performances under the illumination of AM 1.5, 100 mW $cm^{-2}$ for the devices in a structure of ITO/ PEDOT:PSS (40 nm)/ active layer (90-100 nm, 1:1, w/w)/ Ca (20 nm)/ Al (80 nm).

| Active layer | $V_{oc}$ (V) | $J_{sc}$ (mA $cm^{-2}$) | FF (%) | PCE (%) |
|---|---|---|---|---|
| P3HT:P1 | 1.05 | 2.36 | 56.1 | 1.39 |
| P3HT:P2 | 0.74 | 0.85 | 37.3 | 0.23 |
| P3HT:P3 | 1.06 | 0.68 | 38.4 | 0.28 |
| P3HT:P4 | 0.92 | 1.49 | 39.8 | 0.54 |

To further understand the device performance, EQE spectra of the fabricated devices were measured as shown in **Figure 8**. It is observed that all the EQE spectra cover a broad wavelength range from 350 to 650 nm and show a maximum EQE value of 17% at 515 nm, 7.2% at 511 nm, 6.5% at 507 nm, and 13.5% at 554 nm for the OSCs based on P1:P3HT, P2:P3HT, P3:P3HT, and P4:P3HT, respectively. It can be clearly seen that the performance of the devices is well consistent with the results of the EQE measurements. In addition, the calculated $J_{sc}$ values obtained by the integration of the EQE data for the devices agree well with the $J_{sc}$ values obtained from the *J*–*V* measurements. Obviously, the EQE of the devices based on P3HT:P1 is higher than that of the devices based on the blend of P3HT:P2, P3HT:P3, and P3HT:P4, and it can be attributed to the stronger light absorption of P1 and the appropriate film morphology. Such a difference in EQE spectra agrees well with the observed different $J_{sc}$ of the solar cell devices.

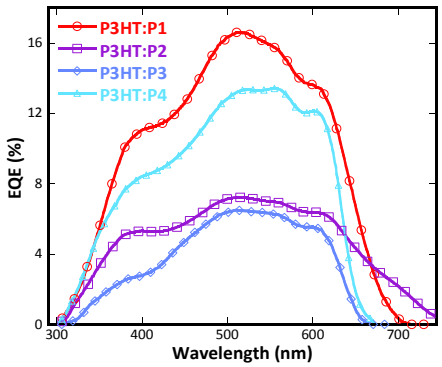


**Figure 8** EQE spectra of the OSC devices in a structure of ITO/ PEDOT:PSS (40 nm)/ active layer (90-100 nm, 1:1, w/w)/ Ca (20 nm)/ Al (80 nm) based on an active layer of P3HT:P1, P3HT:P2, P3HT:P3, and P3HT:P4.

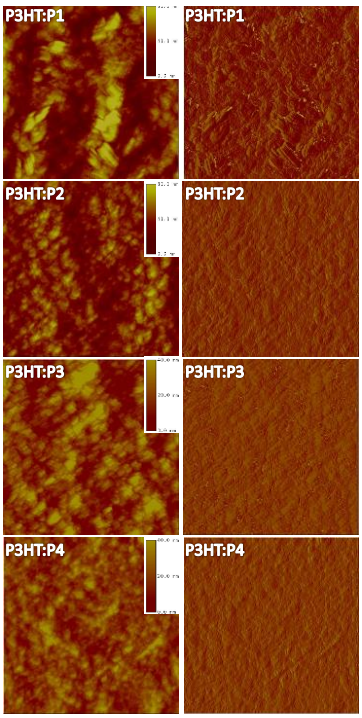


**Figure 9** Tapping mode AFM topography height images ($5 \times 5\ \mu m^2$) (left) and phase images (right) of the blend films of P3HT:P1, P3HT:P2, P3HT:P3, and P3HT:P4.

**Film morphology.** In order to deeply understand the photovoltaic properties of the resulting small molecular materials, the active layer morphology was studied by AFM in the tapping-mode. Similar to the OSC devices, the films for the AFM measurements were also prepared by spin-coating their *o*-dichlorobenzene solutions on top of the PEDOT:PSS layer, which was spin-coated onto the ITO glass substrates. As shown by the topography images presented in **Figure 9**, it can be seen that the different central cores of these four small molecules result in tiny morphology variation in the condensed state. The root-mean-square (rms) roughness of the P3HT:P1, P3HT:P2, P3HT:P3, and P3HT:P4 films are 16.125, 10.118, 10.796, and 7.327 nm, respectively. The blended films exhibit a large roughness, which indicates an unfavourable film morphology that is a major disadvantage for charge separation from the donor to the acceptor, thus leading to lower $J_{sc}$ and FF. It is well-known that the well-defined IPN structure ensures large D–A interfaces and efficient percolation channels for charge transport, thus improving the exciton separation and carrier collection efficiency and leading to a high $J_{sc}$ and FF.

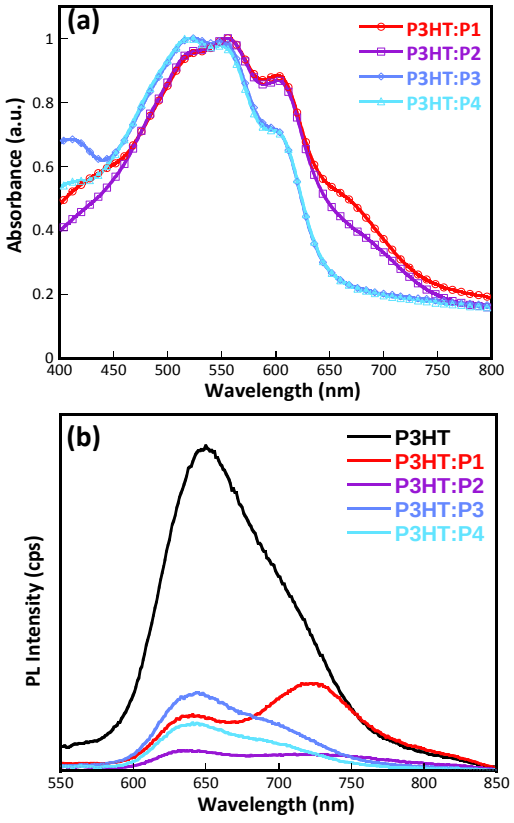


**Figure 10** (a) UV-vis absorption spectra of the blended films P3HT:P1, P3HT:P2, P3HT:P3, and P3HT:P4; (b) PL spectra of the P3HT film and the blend films of P3HT:P1, P3HT:P2, P3HT:P3, and P3HT:P4.

**Photoluminescence characterization.** In order to obtain an insight into the charge transfer process in the donor/acceptor blends, PL spectra of the neat film of P3HT and the blended films of P3HT:P1, P3HT:P2, P3HT:P3, and P3HT:P4 were investigated. The emission spectra were obtained at an excitation wavelength of 520 nm for the films based on P3HT, P3HT:P1, P3HT:P2, P3HT:P3, and P3HT:P4, which is the

strongest absorption wavelength for the P3HT film. As shown in **Figure 10a**, it reveals that these donor-acceptor pairs have well-matched complementary absorption peaks that cover a broad wavelength range from 400 to 700 nm. **Figure 10b** reveals that the PL intensity of the P3HT film is dramatically quenched by the addition of P1, P2, P3, and P4. The results indicate that photo-induced charge transfer from donor to acceptor should be quite efficient to be as an electron acceptor in organic photovoltaic devices. The PL peak of the P1-based blend film at the longer wavelength region should be attributed to the acceptor material P1. AFM images of the P3HT:P1 blend films exhibit feature sizes of about 100 nm, which far exceeds the exciton diffusion length in organic materials, while the blend films of P3HT:P2, P3HT:P3, and P3HT:P4 exhibit relatively small sizes. Although, the PL quenching of P2 is one of the most efficient, the device based on P2 displays very low $J_{sc,}$ which is another factor that contributes to the lower EQE for the P3HT:P2-based OSCs. Probably, a large number of free carriers failed to effectively sweep out and collect at the electrodes prior to recombination.

## Conclusions

In summary, we designed, synthesized and characterized four A-D-A structured novel organic molecules with isoindigo as terminal acceptor units, with different aromatic rigid planar cores such as indacenodithiophene, dithienosilole, anthracene, and pyrene as donor units. These materials exhibit rather high-lying LUMO levels, which is beneficial for achieving high $V_{oc}$. Aside from the good solubility and stability, effective PL quenching was observed when P3HT is blended with the developed acceptor molecules, indicating efficient charge/energy transfer occurred and the four materials could be used as acceptors in solution-processable organic solar cells. Compared with P2, P3 and P4, a PCE of 1.39% was achieved for the OSCs based on P1 as the acceptor material and P3HT as the donor material (1:1, w/w) without additive and post-deposition annealing of the active layers, which is the highest value for the polymer BHJ OSCs based on isoindigo small molecules as non-fullerene acceptors. This current result demonstrates that isoindigo unit combining different donors with an A-D-A structure, which consists of conjugated donor backbone and acceptor terminal units, could be a useful building block for the development of promising acceptor materials for OSCs. Process optimization plays a central role in the realization of high-performance non-fullerene organic solar cells. Careful optimizations of the film morphologies by varying the blend ratios, thermal annealing conditions, active layer thicknesses, changing the spin-coating solvents with different boiling-points, and accompanying with the utilizations of high boiling-point cosolvent may be effective route toward highly efficient non-fullerene organic solar cells.

## Acknowledgements

The authors greatly appreciate the financial support from the Ministry of Science and Technology (2014CB643501, 2015CB655003 and 2014DFA52030) and the National Natural Science Foundation of China (91233116, 51573059 and 51073057).

## References

1 G. Yu, J. Gao, J. C. Hummelen, F. Wudl, A. J. Heeger, Science, 1995, 270, 1789.
2 H. Y. Chen, J. H. Hou, S. Q. Zhang, Y. Y. Liang, G. W. Yang, Y. Yang, L. P. Yu, Y. Wu, G. Li, Nat. Photon., 2009, 3, 649.
3 X. G. Guo, N. J. Zhou, S. J. Lou, J. Smith, D. B. Tice, J. W. Hennek, R. P. Ortiz, J. T. L. Navarrete, S. Y. Li, J. Strzalka, L. X. Chen, R. P. H. Chang, A. Facchetti, T. J. Marks, Nat. Photon., 2013, 7, 825.
4 Z. C. He, C. M. Zhong, S. J. Su, M. Xu, H. B. Wu, Y. Cao, Nat. Photon., 2012, 6, 591.
5 J. B. You, L. T. Dou, K. Yoshimura, T. Kato, K. Ohya, T. Moriarty, K. Emery, C. C. Chen, J. Gao, G. Li, Y. Yang, Nat. Commun., 2013, 4, 1446.
6 B. Parida, S. Iniyan, R. Goic, Renew Sust. Energ. Rev., 2011, 15, 1625.
7 J. D. Myers, J. Xue, Polym. Rev., 2012, 52, 1.
8 S. H. Liao, H. J. Jhuo, Y. S. Cheng, S. A. Chen, Adv. Mater., 2013, 25, 4766.
9 L. Ye, W. Zhang, H. Zhao, J. Hou, Chem. Mater., 2014, 26, 3603.
10 C.-Z. Li, C.-Y. Chang, Y. Zang, H.-X. Ju, C.-C. Chueh, P.-W. Liang, N. Cho, D. S. Ginger, A. K. Y. Jen, Adv. Mater., 2014, 26, 6262.
11 Y. He, Y. Li, Phys. Chem. Chem. Phys., 2011, 13, 1970.
12 A. Anctil, C. W. Babbitt, R. P. Raffaelle, B. J. Landi, Environ. Sci. Technol., 2011, 45, 2353.
13 C.-W. Ge, C.-Y. Mei, J. Ling, J.-T. Wang, J.-T. Wang, F.-G. Zhao, L. Liang, H.-J. Li, Y.-S. Xie, W.-S. Li, J. Polym. Sci., A, 2014, 52, 1200.
14 C.-W. Ge, C.-Y. Mei, J. Ling, F.-G. Zhao, H.-J. Li, L. Liang, J.-T. Wang, J.-C. Yu, W. Shao, Y.-S. Xie, W.-S. Li, J. Polym. Sci., A, 2014, 52, 2356.
15 X. Zhang, Z. Lu, L. Ye, C. Zhan, J. Hou, S. Zhang, B. Jiang, Y. Zhao, J. Huang, S. Zhang, Y. Liu, Q. Shi, Y. Liu, J. Yao, Adv. Mater., 2013, 25, 5791.
16 W. Jiang, L. Ye, X. G. Li, C. Y. Xiao, F. Tan, W. C. Zhao, J. H. Hou, Z. H. Wang, Chem. Commun., 2014, 50, 1024.
17 Z. H. Lu, B. Jiang, X. Zhang, A. L. Tang, L. L. Chen, C. L. Zhan, J. N. Yao, Chem. Mater., 2014, 26, 2907.
18 Y. Lin, Y. Wang, J. Wang, J. Hou, Y. Li, D. Zhu, X. Zhan, Adv. Mater., 2014, 26, 5137.
19 J. T. Bloking, T. Giovenzana, A. T. Higgs, A. J. Ponec, E. T. Hoke, K. Vandewal, S. Ko, Z. Bao, A. Sellinger, M. D. McGehee, Adv. Energy Mater., 2014, 4, 1301426.
20 L. Ye, W. Jiang, W. Zhao, S. Zhang, D. Qian, Z. Wang, J. Hou, Small, 2014, 22, 4658.
21 Z. Mao, W. Senevirathna, J.-Y. Liao, J. Gu, S. V. Kesava, C. Guo, E. D. Gomez, G. Sauvé, Adv. Mater., 2014, 26, 6290.
22 Y. Zang, C. Z. Li, C. C. Chueh, S. T. Williams, W. Jiang, Z. H. Wang, J. S. Yu, A. K. Jen, Adv. Mater., 2014, 26, 5708.
23 J. Zhao, Y. Li, H. Lin, Y. Liu, K. Jiang, C. Mu, T. Ma, J. Y. L. Lai, H. Yan, Energy Environ. Sci., 2015, 8, 520.
24 X. Zhang, C. L. Zhan, J. Yao, Chem. Mater., 2015, 27, 166.
25 T. Kim, J. H. Kim, T. E. Kang, C. Lee, H. Kang, M, Shin, C. Wang, B. Ma, U. Jeong, T.-S. Kim, B. Kim, Nat. Commun., 2015, DOI: 10.1038/ncomms9547.
26 Y. Zhong, M. T. Trinh, R. S. Chen, G. E. Purdum, P. P. Khlyabich, M. Sezen, S. Oh, H. Zhu, B. Fowler, B. Zhang, W. Wang, C.-Y. Nam, M. Y. Sfeir, C. T. Black, M. L. Steigerwald,



 

Y.-L. Loo, F. Ng, X.-Y. Zhu, C. Nuckolls, Nat. Commun., 2015, DOI: 10.1038/ncomms9242.
27 Y.-J. Hwang, H. Y. Li, B. A. E. Courtright, S. Subramaniyan, S. A. Jenekhe, Adv. Mater., DOI: 10.1002/adma.201503801.
28 B. Walker, C. Kim, T.-Q. Nguyen, Chem. Mater., 2010, 23, 470.
29 Y. Li, L. Xue, H. Li, Z. Li, B. Xu, S. Wen, W. Tian, Macromolecules, 2009, 42, 4491.
30 E. Steingruber, in Ullmanns Encycl. Ind. Chem. Wiley-VCH Verlag GmbH & Co. KGaA, 2000.
31 R. Stalder, J. Mei, K. R. Graham, L. A. Estrada, J. R. Reynolds, Chem. Mater., 2014, 26, 664.
32 T. Maugard, E. Enaud, P. Choisy, M. D. Legoy, Phytochemistry, 2001, 58, 897.
33 R. Stalder, J. Mei, J. R. Reynolds, Macromolecules, 2010, 43, 8348.
34 W. Elsawy, C.-L. Lee, S. Cho, S.-H. Oh, S.-H. Moon, A. Elbarbary, J.-S. Lee, Phys. Chem. Chem. Phys., 2013, 15, 15193.
35 T. Lei, J.-Y. Wang, J. Pei, Acc. Chem. Res., 2014, 47, 1117.
36 E. Wang, W. Mammo, M. R. Andersson, Adv. Mater., 2014, 26, 1801.
37 C.-C. Ho, C.-A. Chen, C.-Y. Chang, S. B. Darling, W.-F. Su, J. Mater. Chem. A, 2014, 2, 8026.
38 J. Areephong, R. R. S. Juan, A.-J. Payne, G. C. Welch, New J. Chem., 2015, 39, 5075.
39 P. Sonar, G.-M. Ng, T. T. Lin, A. Dodabalapur, Z.-K. Chen, J. Mater. Chem., 2010, 20, 3626.
40 D. Chandran, K.-S. Lee, Macromol. Res., 201 3, 21, 272.
41 M. Chen, W. Fu, M. Shi, X. Hu, J. Pan, J. Ling, H. Li, H. Chen, J. Mater. Chem. A, 2012, 1, 105.
42 S. Loser, C. J. Bruns, H. Miyauchi, R. P. Ortiz, A. Facchetti, S. I. Stupp, T. J. Marks, J. Am. Chem. Soc., 2011, 133, 8142.
43 Y. Lin, L. Ma, Y. Li, Y. Liu, D. Zhu, X. Zhan, Adv. Energy Mater., 2013, 3, 1166.
44 L. A. Estrada, R. Stalder, K. A. Abboud, C. Risko, J.-L. Bradas, J. R. Reynolds, Macromolecules, 2013, 46, 8832.
45 S. M. McAfee, J. M. Topple, A. J. Payne, J. P. Sun, I. G. Hill, G. C. Welch, ChemPhysChem., 2015, 16, 1190.
46 S. M. McAfee, J. M. Topple, A. J. Payne, J. P. Sun, I. G. Hill, G. C. Welch, RSC Adv., 2015, 5, 80098.
47 X. Liu, Y. Xie, H. B. Zhao, X. Y. Cai, H. B. Wu, S.-J. Su, Y. Cao, New J. Chem., 2015, 39, 8771.
48 C. P. Chen, S. H. Chan, T. C. Chao, C. Ting and B. T. Ko, J. Am. Chem. Soc., 2008, 130, 12828.
49 P. M. Beaujuge, H. N. Tsao, M. R. Hansen, C. M. Amb, C. Risko, J. Subbiah, K. R. Choudhury, A. Mavrinskiy, W. Pisula, J.-L. Brédas, F. So, K. Müllen, and J. R. Reynolds, J. Am. Chem. Soc., 2012, 134, 8944.
50 C. Yang, J. Jacob, and K. Müllen, Macromolecules, 2006, 39, 5696.
51 T. M. Figueira-Duarte, P. G. D. Rosso, R. Trattnig, S. Sax, E. J. W. List, and K. Müllen, Adv. Mater., 2010, 22, 990.
52 E. Wang, Z. Ma, Z. Zhang, P. Henriksson, O. Inganas, F. Zhang, M. R. Andersson, Chem. Commun., 2011, 47, 4908.
53 E. Zhou, J. Cong, K. Tajima, K. Hashimoto, Chem. Mater., 2010, 22, 4890.

## TOC Graphic

**Title:** Synthesis and Photovoltaic Properties of A-D-A Type Non-fullerene Acceptors Containing Isoindigo Terminal Units

**Authors:** Xin Liu, Yuan Xie, Xinyi Cai, Yunchuan Li, Hongbin Wu, Shi-Jian Su, Yong Cao

**Abstract:** Four solution-processable acceptor-donor-acceptor structured organic molecules with isoindigo as terminal acceptor units and different aromatic rigid planar cores as donor units were designed and synthesized as the acceptor materials in organic solar cells (OSCs).